Response of Sea Ice to the Arctic Oscillation

IGNATIUS G. RIGOR

Applied Physics Laboratory and Department of Atmospheric Sciences, University of Washington, Seattle, Washington

JOHN M. WALLACE

Department of Atmospheric Sciences, University of Washington, Seattle, Washington

ROGER L. COLONY

Frontier Research System for Global Change, International Arctic Research Center, University of Alaska, Fairbanks, Alaska

(Manuscript received 18 April 2001, in final form 10 April 2002)

ABSTRACT

Data collected by the International Arctic Buoy Programme from 1979 to 1998 are analyzed to obtain statistics of sea level pressure (SLP) and sea ice motion (SIM). The annual and seasonal mean fields agree with those obtained in previous studies of Arctic climatology. The data show a 3-hPa decrease in decadal mean SLP over the central Arctic Ocean between 1979–88 and 1989–98. This decrease in SLP drives a cyclonic trend in SIM, which resembles the structure of the Arctic Oscillation (AO).

Regression maps of SIM during the wintertime (January–March) AO index show 1) an increase in ice advection away from the coast of the East Siberian and Laptev Seas, which should have the effect of producing more new thin ice in the coastal flaw leads; 2) a decrease in ice advection from the western Arctic into the eastern Arctic; and 3) a slight increase in ice advection out of the Arctic through Fram Strait. Taken together, these changes suggest that at least part of the thinning of sea ice recently observed over the Arctic Ocean can be attributed to the trend in the AO toward the high-index polarity.

Rigor et al. showed that year-to-year variations in the wintertime AO imprint a distinctive signature on surface air temperature (SAT) anomalies over the Arctic, which is reflected in the spatial pattern of temperature change from the 1980s to the 1990s. Here it is shown that the memory of the wintertime AO persists through most of the subsequent year: spring and autumn SAT and summertime sea ice concentration are all strongly correlated with the AO index for the previous winter. It is hypothesized that these delayed responses reflect the dynamical influence of the AO on the thickness of the wintertime sea ice, whose persistent ''footprint'' is reflected in the heat fluxes during the subsequent spring, in the extent of open water during the subsequent summer, and the heat liberated in the freezing of the open water during the subsequent autumn.

1. Introduction

Dramatic changes in Arctic climate have been noted during the past two decades. Walsh et al. (1996) reported a 5-hPa decrease in sea level pressure (SLP) over the central Arctic Ocean between the periods 1986–94 and 1979–85. Rigor et al. (2000) found warming trends in surface air temperature (SAT) over the Arctic Ocean during winter and spring, with values as high as 2°C decade^{-1} in the eastern Arctic during spring. These changes have been linked to changes in the Arctic Oscillation (AO), whose index is defined as the leading principal component (PC) of Northern Hemisphere SLP (Thompson and Wallace 1998). The AO can be characterized as an exchange of atmospheric mass between the Arctic Ocean and the surrounding zonal ring centered ~45°N. The observed trend in the AO toward its ''high index'' polarity (i.e., toward stronger westerlies at subpolar latitudes and lower SLP over the Arctic) is a way of interpreting the observed decrease in SLP over the North Pole and the associated cyclonic tendency in the surface winds over the Arctic. In this study, we show how the changes in surface wind associated with the fluctuations and trend in the AO affect sea ice motion (SIM) in the central Arctic and how the changes in SIM, in turn, affect the thickness and concentration of sea ice, and the distribution of SAT over the Arctic.

The SIM affects the distribution of latent and sensible heat flux by the convergence and divergence of sea ice. The convergence of ice produces thicker ice by rafting ice floes on top of each other or by producing pressure ridges; thicker sea ice insulates the atmosphere from the

Corresponding author address: Ignatius G. Rigor, Applied Physics Laboratory, University of Washington, 1013 N.E. 40th St., Seattle, WA 98105-6698.
E-mail: ignatius@atmos.washington.edu

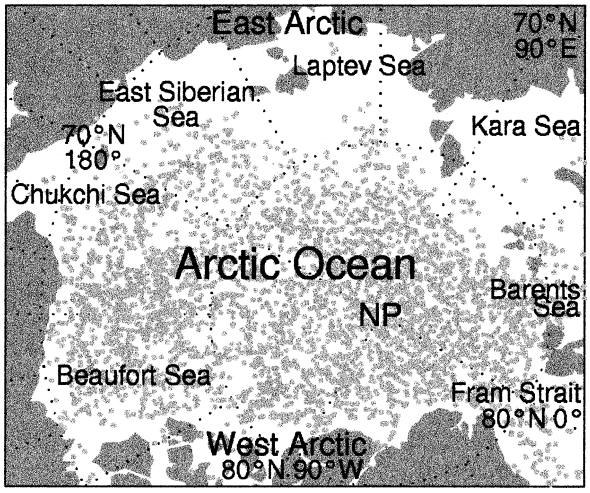

FIG. 1. Monthly buoy positions from 1979 to 1998. The locations of the geographical areas mentioned in the text are also shown.

ocean. The divergence of ice produces more open water and thin ice where heat from the ocean can escape to the atmosphere. The extra heat released in regions of divergence may prolong the melt season, when the surface albedo is relatively low, thereby increasing the annually integrated absorption of solar radiation. Changes in SIM may affect summer sea ice concentration (SIC), which is important for navigation, and may have implications for the transport of sediments and pollutants across the Arctic. Most of the sea ice formed in the Arctic Ocean is exported through Fram Strait into the Greenland Sea and to the North Atlantic where the ice may affect the global thermohaline circulation.

The primary datasets used in this study were obtained from the International Arctic Buoy Programme (IABP), which has maintained a network of buoys drifting on the pack ice of the Arctic Ocean since 1979. These buoys carry instruments for measuring SLP, SAT, and other geophysical quantities. Sea ice motion is estimated from the sequence of station positions as monitored by the Argos satellite system. In this study 20 yr of IABP data from 1979 to 1998 are used.

Section 2 describes the datasets and analysis procedures used in this study in more depth. Section 3 presents an abridged seasonal climatology of SLP and SIM estimated from the IABP data. Section 4 documents the interdecadal trends in SLP and SIM. Section 5 shows the signature of the AO on the trends in SLP and SIM. In sections 6–8, we discuss some implications of these changes for Arctic climate.

2. Data

The primary datasets used in this study are SLP, SAT, and SIM from the IABP. The monthly positions of the buoys from 1979 to 1998 and some geographic locations mentioned in this study are shown in Fig. 1. During this period more than 500 buoys were deployed, most of which had lifetimes of ~2 yr. At any given time there were 20–30 buoys drifting on the Arctic pack ice, with a spacing of roughly 300–600 km. The buoy data are transmitted to and collected by the Argos satellite system, which also calculates the positions of the buoys with a standard error of ≤300 m. The measurement errors are ~0.1°C for SAT and ≤1 hPa for SLP. The SLP, SIM, and SAT data used in this study were obtained from the IABP Web server (available online at http://iapb.apl.washington.edu) and are archived as the International Arctic Ocean Buoy Data Products at the National Snow and Ice Data Center (World Data Center–A). The IABP dataset is by far the largest compilation of direct observations of SAT, SLP, and SIM for the Arctic.

The SLP observations from the buoys were combined with the SLP fields derived from the National Center for Environmental Prediction (NCEP) reanalysis obtained from the National Center for Atmospheric Research (NCAR; NCEP–NCAR datasets DS 82.0 and 83.0), using optimal interpolation [OI; see Thorndike and Colony (1982) for details]. Over the Arctic Ocean near the buoys, estimates of SLP are based primarily on the buoy observations, but away from the buoy network, the estimates are based on the NCEP–NCAR analysis.

Monthly estimates of SIM were calculated from the displacements of the buoys during each month. Given the positioning error of the Argos system (300 m), the observation error of monthly ice velocity is estimated to be ≤ 0.02 cm s^{-1}. Monthly gridded fields of SIM were analyzed using the OI scheme of Pfirman et al. (1997), which combined the observed ice motions with geostrophic winds to supplement the analysis where the buoy data were sparse (see Fig. 1). In the present study, the SIM fields were based solely on the observed SIM in order to distinctly show how the changes in SIM relate to the changes in atmospheric circulation. The OI scheme uses a mean field based on binned averages of the observations near each grid point and a correlation length scale of 1300 km (Pfirman et al. 1997).

The SAT data used in this study are based on the IABP–POLES (Polar Exchange at the Sea Surface) SAT analysis described in Rigor et al. (2000). This dataset combines the observations from the buoys, with data from manned drifting stations and meteorological land stations, also using OI (Rigor et al. 2000). This paper also discusses the accuracy of the buoy SAT observations, and how these data were corrected for use in the IABP–POLES SAT analysis.

Sea ice concentration and ice chart data were also used in this study. The SIC data were derived from Special Sensor Microwave Imager (SSM/I) and the Scanning Multichannel Microwave Radiometer (SMMR) satellites using the bootstrap algorithm. These data were obtained from the earth observing system Distributed Active Archive Center at the National Snow and Ice Data Center (NSIDC), University of Colorado

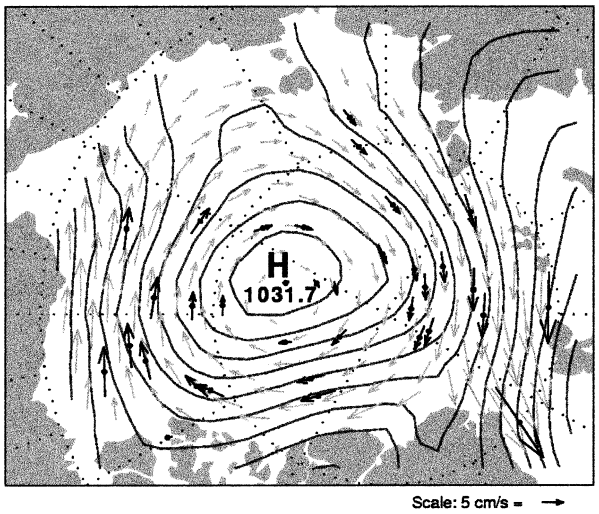

FIG. 2. Analyzed fields of SLP and SIM for Dec 1993. Dots mark positions of IABP buoys, and arrows show buoy velocities. Contours are shown every 2 hPa.

at Boulder. The ice chart data [sea-ice data on a digital grid (SIGRID)] were produced by the Arctic and Antarctic Research Institute in St. Petersburg, and were also obtained from NSIDC.

Figure 2 shows the analyzed fields of SLP and SIM for December 1993. For comparison, the buoy positions during that month are marked with dots, and the buoy velocities are shown as black arrows. (Analogous plots for other periods can be obtained from the IABP Web server.) This figure shows the strong correspondence between SLP and SIM noted by Thorndike and Colony (1982), who found that geostrophic winds account for more than 70% of the variance in daily SIM.

3. Climatology

The mean (1979–98) fields of SLP and SIM for winter (January–March) and summer (July–September) shown in Fig. 3 exhibit some well-known features of Arctic climate such as the Beaufort high in SLP, which drives the anticyclonic Beaufort gyre in SIM, and the Transpolar Drift Stream (the zone of high ice velocity across the Arctic Ocean toward Fram Strait). The winter field of SIM exhibits an export of ice into the East Siberian Sea from the Arctic Ocean, and import of ice from the Laptev and Kara Seas into the Arctic Ocean. The main sink of ice from the Arctic Ocean is through Fram Strait. In the annual mean, 900 000 km^2 of ice flow through Fram Strait to the North Atlantic (Colony and Thorndike 1984). The SIM map for summer exhibits a cyclonic gyre in the eastern Arctic associated with a low in the SLP field. Although the Beaufort high is much weaker during the summer and has retreated onto land over Alaska, the mean field of SIM in the Beaufort Sea remains anticyclonic. The fields for the transition seasons (not shown) resemble the winter climatology.

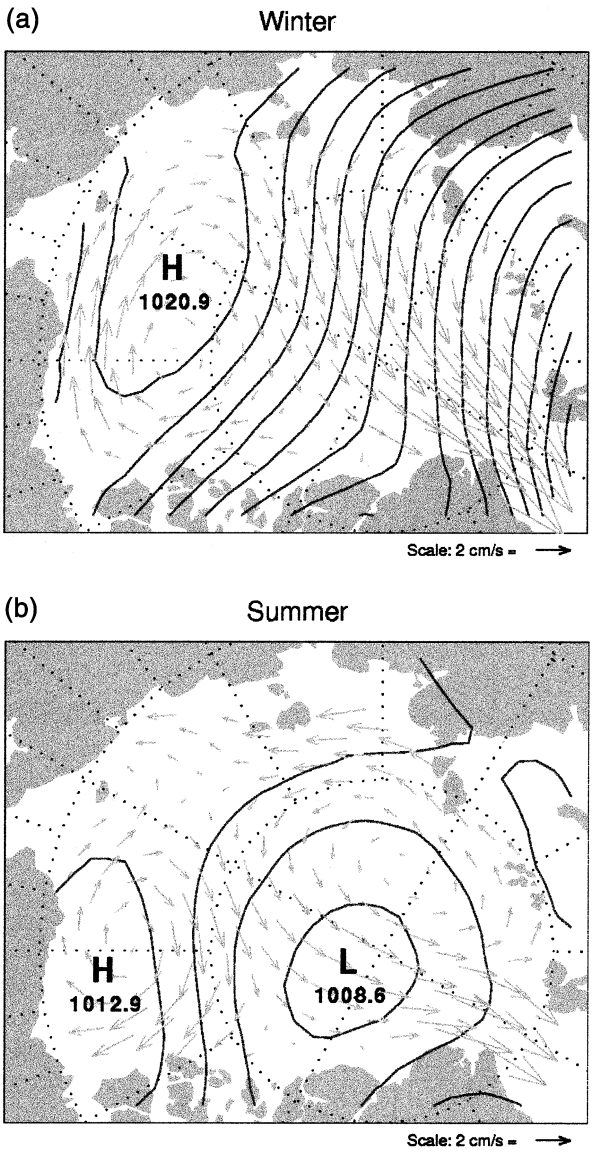

FIG. 3. Seasonal mean fields of SLP and SIM for 1979–98: (a) winter and (b) summer.

The drift of sea ice across the isobars in these long-term means (Fig. 3) reflects the influence of the ocean currents upon SIM. On timescales longer than a year the contributions from the winds and ocean currents in driving SIM are roughly equal, but as shown in Fig. 2, the drift of sea ice on shorter timescales ($\leq$1 yr) follows the wind (Thorndike and Colony 1989). On short timescales SIM can be approximated by the simple rule of thumb that the ice drifts with a speed of about 1% of and 5° to the right of the geostrophic winds (e.g., Thorndike and Colony 1982; Zubov 1943). And as noted by Aagaard (1989), the drift of sea ice and the surface ocean currents are decoupled from the deeper currents of the Arctic Ocean, which tend to flow counterclockwise, opposite to the flow at the surface.

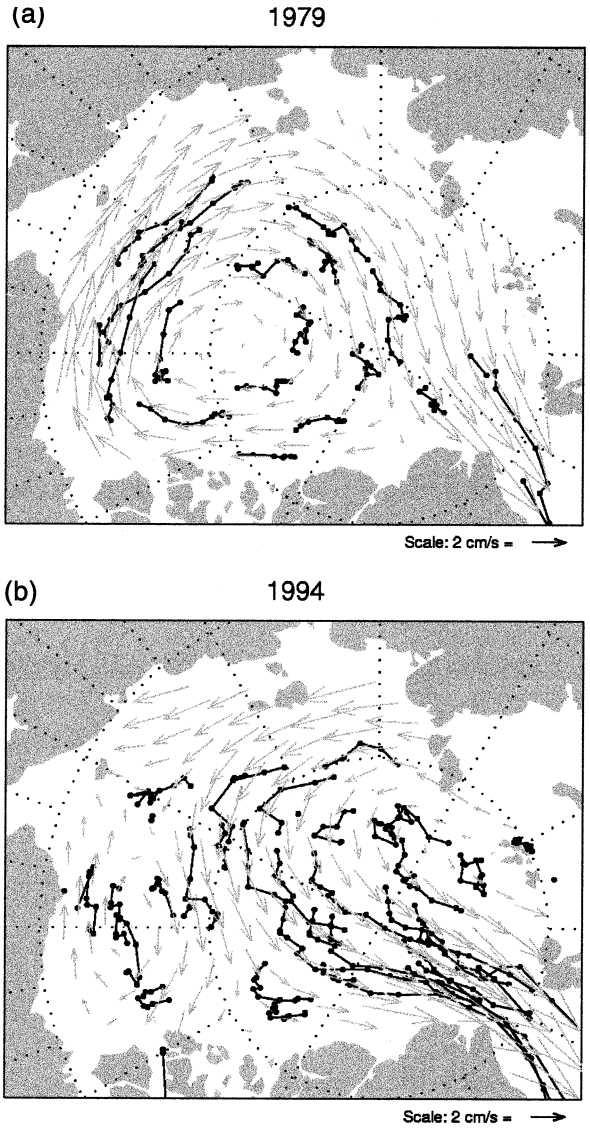

FIG. 4. Analyzed fields of SIM for (a) 1979 and (b) 1994 (gray vectors). The monthly positions of the buoys are also shown. Trajectories for individual buoys are indicated by black lines.

4. Interdecadal trends in SLP and SIM

Figure 4 shows the analyzed mean fields of SIM (gray vectors) for the contrasting years 1979 and 1994. The monthly drift trajectories of the buoys during the 2 yr are also plotted (black lines) to show how well the analyzed SIM field captures the observed drift. During 1979 the basic features shown in the climatology were evident, but the Beaufort gyre covered a larger area and the Transpolar Drift Stream was shifted farther toward the eastern side of the Arctic Ocean. During 1994, the Beaufort gyre was reduced in size, there was a large cyclonic circulation north of the Kara Sea (85°N, 90°E), and the Transpolar Drift Stream was shifted to the western Arctic and passed directly across the central Arctic and the North Pole. Less recirculation was evident in the Beaufort gyre, and the ice velocities through Fram Strait were higher.

Following the procedure of Walsh et al. (1996), but using a 25% longer record, we separated the 20 yr of data into the first (1979–88) and second (1989–98) decades and computed the difference between them, as shown in Fig. 5. Compared with 1979–88 (Fig. 5a), 1989–98 (Fig. 5b) shows a 2-hPa reduction in the central SLP of the Beaufort high, a corresponding reduction in the strength of the Beaufort gyre, and a shift of the Transpolar Drift Stream toward the west. Over the central Arctic the drops in SLP (Fig. 5c) are 2–4 hPa, and the associated cyclonic tendency in the atmospheric circulation drives a cyclonic tendency in SIM.

Figure 6 shows the winter and summer mean fields of SLP and SIM for both decades. The winter fields are very similar to but stronger than the annual mean fields shown in the previous figure. The SLP decrease from the first to the second decade is much larger during winter (3–6 hPa) than during summer (1–2 hPa), yet the cyclonic summer tendency in SIM is as large or larger than the winter tendency. This higher sensitivity of the summer SIM to the geostrophic wind forcing can be attributed to the lower internal stress of the summer ice pack.

5. The Arctic Oscillation signature in SLP and SIM

To show the changes in SIM that occur in response to changes in the amplitude and polarity of the AO, the monthly SIM fields were regressed onto the AO index (i.e., the standardized leading PC of the monthly SLP based on all calendar months), whose time series is shown in Fig. 7. These data were obtained from the annular modes Web site at http://horizon.atmos.colostate.edu/ao/. The index varies almost randomly from month to month, with a 1-month lag correlation of only 0.35. The step toward higher values of the index in 1989 coincides with the changes in circulation noted by Walsh et al. (1996) and conveniently separates the two decades of data used in this study. Although the AO and the North Atlantic Oscillation (NAO, e.g., Hurrell 1995) indices are highly correlated, the AO index is used in this study because it captures more of the hemispheric, as opposed to the regional (North Atlantic/European), variability in the atmospheric circulation (Thompson and Wallace 1998). This distinction is important because many of the changes in Arctic climate noted in the introduction occur in the Laptev, East Siberian, and Chukchi Seas, far from the Icelandic center of action of the NAO.

Regressions maps of the monthly mean fields of SLP and SIM onto the AO index for winter and summer seasons, shown in Figs. 8a and 8b, resemble the decadal difference fields shown in Figs. 6c and 6f; that is, they are dominated by cyclonic anomalies in the SLP and

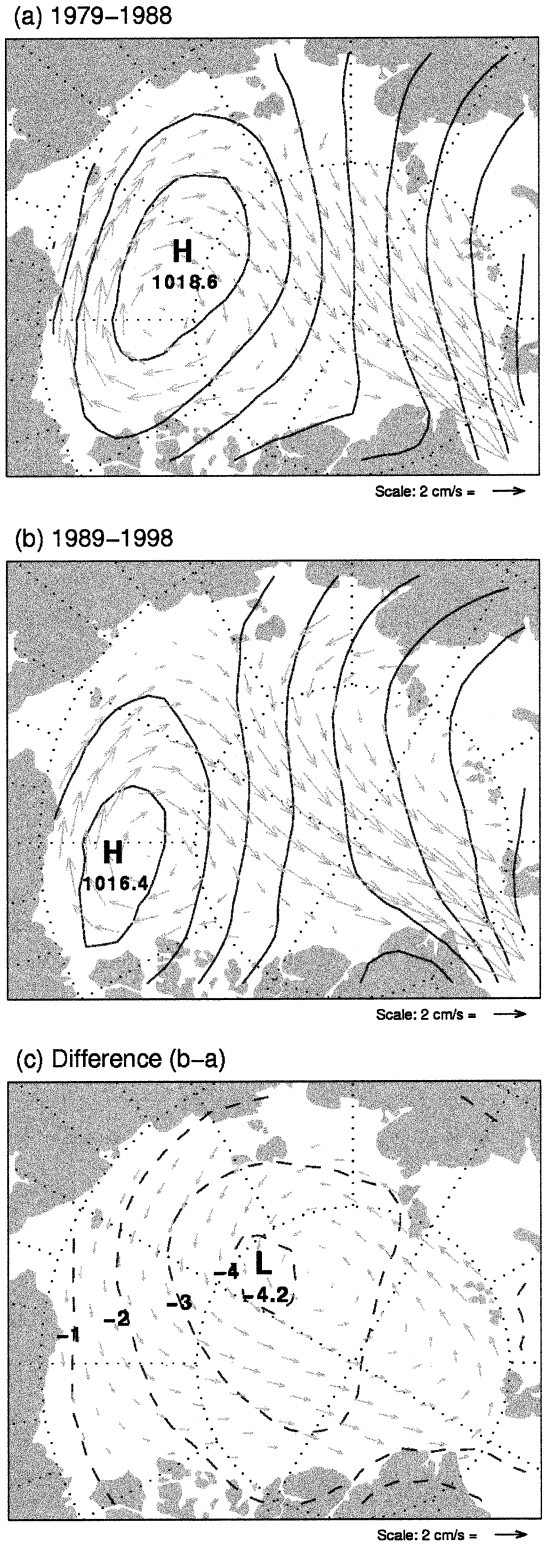

FIG. 5. Mean fields of SIM and SLP for the two decades studied: (a) 1979–88, (b) 1989–98, and (c) difference [(a) − (b)].

SIM fields. Sea level pressures over the Arctic are lower by 3–5 hPa, and the SIM is more cyclonic during the high-index phase of the AO. The SLP anomalies are stronger during winter, the most active season of the AO, but the SIM anomalies are roughly comparable in the two seasons.

The correlations between SIM (in the direction parallel to the regression vectors) and the AO during winter range from ~0.35 near Fram Strait to ~0.40 in the Chukchi and Beaufort Seas. During summer the correlations are ~0.30 throughout most of the basin. The 95% confidence limit based a two-sided Student's *t* test, a null hypothesis of zero correlation, with ~48 degrees of freedom [one for each month, and reduced in accordance with the observed month-to-month autocorrelation (Leith 1973)], is ~0.25. Hence, the correlations are statistically significant wherever speeds are >0.5 cm s^{-1}. All the features described below satisfy that criterion.

Regression maps of the mean fields of SLP and SIM on the NAO index for winter exhibit similar features (Fig. 8c), but the patterns over the central Arctic Ocean are weaker than the corresponding patterns based on the AO. The differences at Fram Strait are small, but the stronger cyclonic AO anomaly in SLP in the central Arctic basin drives a stronger (~1 cm s^{-1}) cyclonic anomaly in ice motion in the East Siberian, Chukchi, and Beaufort Seas. The AO explains 52% of the variance of SLP over the Arctic Ocean during winter and 36% during summer, whereas the NAO explains only 22% during winter and 3% during summer. These differences have implications for the changes in sea ice thickness and concentration discussed in section 6.

Composite maps of the mean SLP and SIM fields during low-index (−1 standard deviation) and high-index (+1 standard deviation) states of the AO, constructed by simply adding and subtracting the regression fields (Fig. 8) to the mean fields (Fig. 3), are shown in Fig. 9. Note the similarity of the low-index maps (Fig. 9 top) to the first decade of buoy data (Fig. 6 top row) and the similarity of the high-index maps (Fig. 9 bottom) to the second decade of buoy data (Fig. 6 middle row). Relative to low-index winters, the high-index winters show a weaker Beaufort high, a much reduced Beaufort gyre, and a westward shifted Transpolar Drift that cuts across the center of the Arctic Ocean and the North Pole. This shift is accompanied by a stronger cyclonic circulation to the north of the Kara and Laptev Seas. During summer, the high-index map captures the stronger cyclonic anomalies in SLP and SIM that are characteristic of the second summer decade of the 20-yr record (Fig. 6e).

The difference fields from the first to the second decade (Figs. 6c and 6f) and the regression maps of SLP and SIM upon the AO index (Fig. 8) exhibit the decline in SLP over the Arctic Ocean first noted by Walsh et al. (1996). The SIM anomaly is qualitatively consistent with the change in atmospheric circulation. The regres-

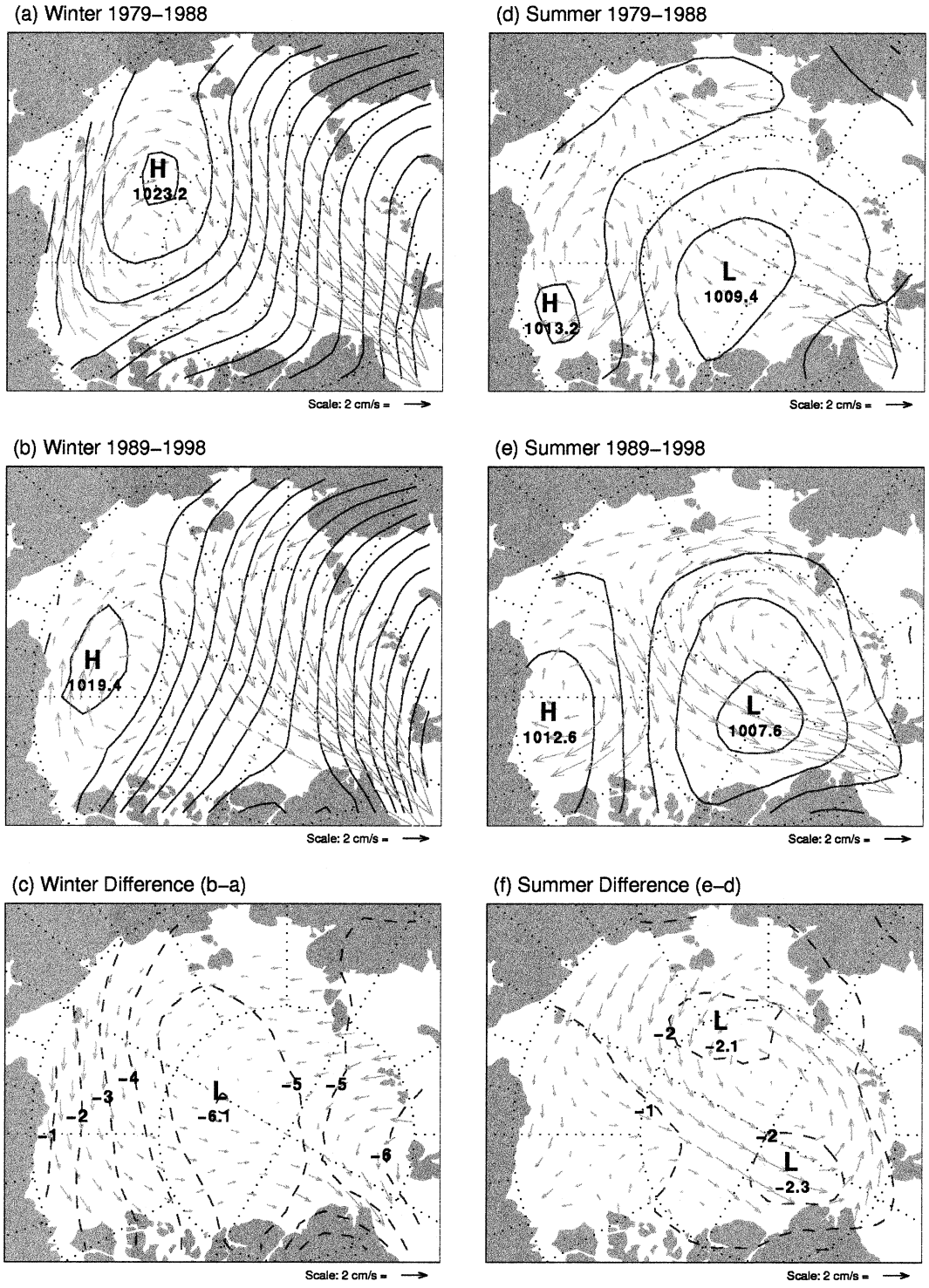

FIG. 6. Mean fields of SIM and SLP for winter and summer for the two decades studied. (a) Winter 1979–88, (b) winter 1989–98, (c) winter difference [(b) − (a)], (d) summer 1979–88, (e) summer 1989–98, and (f) summer difference [(e) − (d)].

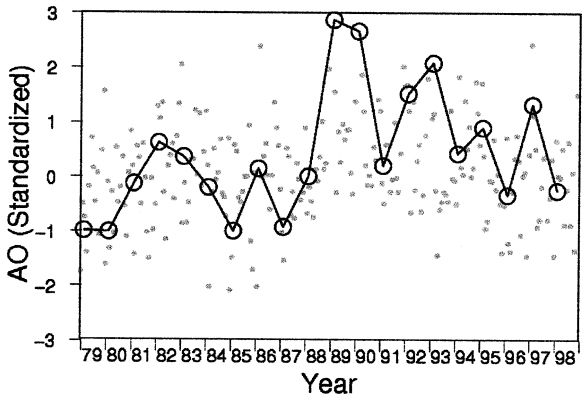

FIG. 7. Standardized monthly AO index (dots) and winter means of the monthly AO index (circles) for 1979–98.

sion map for the winter months shows less export of ice into the East Siberian Sea, much less advection of ice from the Beaufort Sea and western Arctic into the eastern Arctic, and slightly more advection of ice through Fram Strait. Figure 8 also shows that during summer the AO does not affect the ice flux through Fram Strait. Although the circulation is cyclonic throughout most of the central Arctic Ocean during high-index summer months, a weakened Beaufort gyre still persists. Only during extreme high-index phase of the AO (+2 standard deviation, or less than 2.5% of the time) does the circulation in the Arctic become predominantly cyclonic.

The existence of two regimes of SIM has long been discussed in the literature (e.g., Proshutinsky and Johnson 1997; Gudkovich 1961). Figures 10a and 10b show SIM circulation regimes proposed by Gudkovich (1961) as adapted from Fig. 4 of Proshutinsky and Johnson (1997). Also shown (Figs. 10c and 10d) are composite maps of SIM for high- and low-index polarities of the AO for all months of the year. They show comparable locations for the Transpolar Drift Stream and similar changes in the size of the Beaufort gyre. However, the SIM data indicate that the cyclonic circulations north of the Laptev Sea are not closed gyres in either phase, and they show an export (Fig. 10a), rather than an import (Fig. 10c) of ice from the East Siberian Sea during the

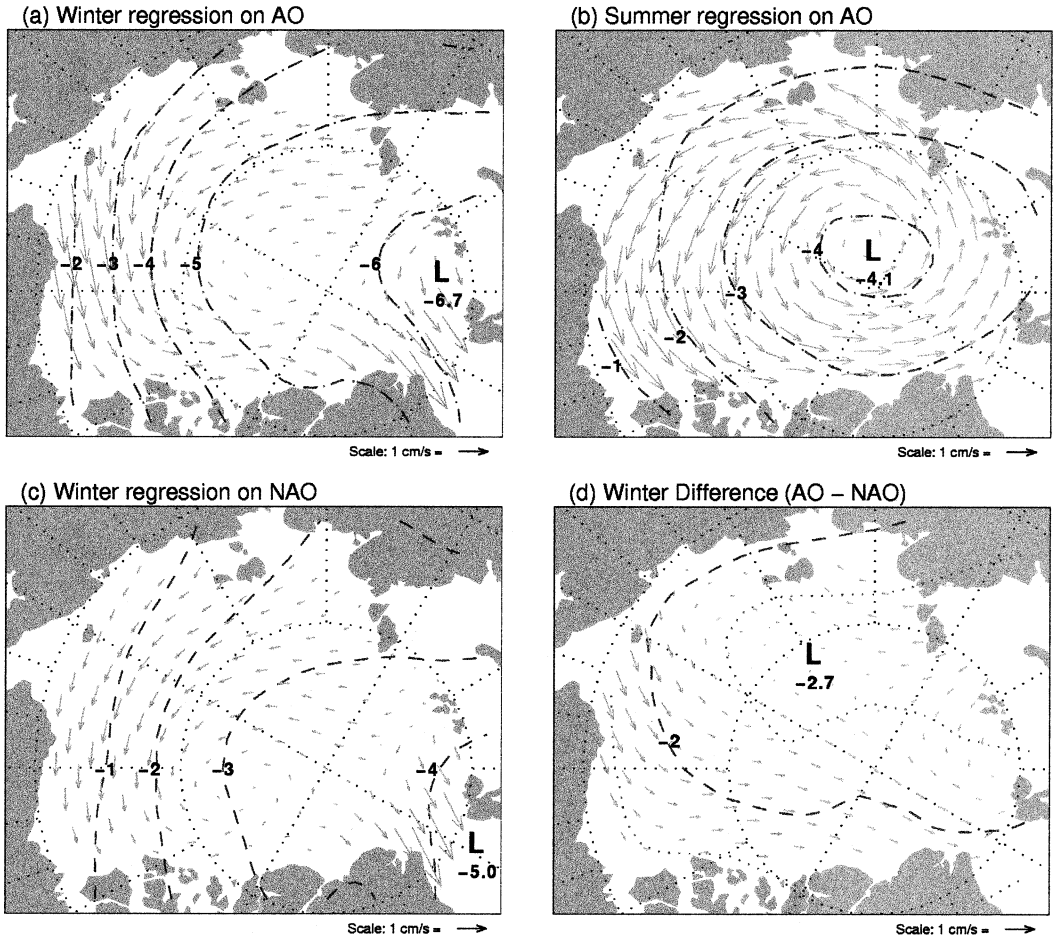

FIG. 8. Regression maps of SLP and SIM. Regressions on the AO for (a) winter and (b) summer. (c) Regressions on the NAO for winter. (d) The difference between the winter AO and NAO regression maps.

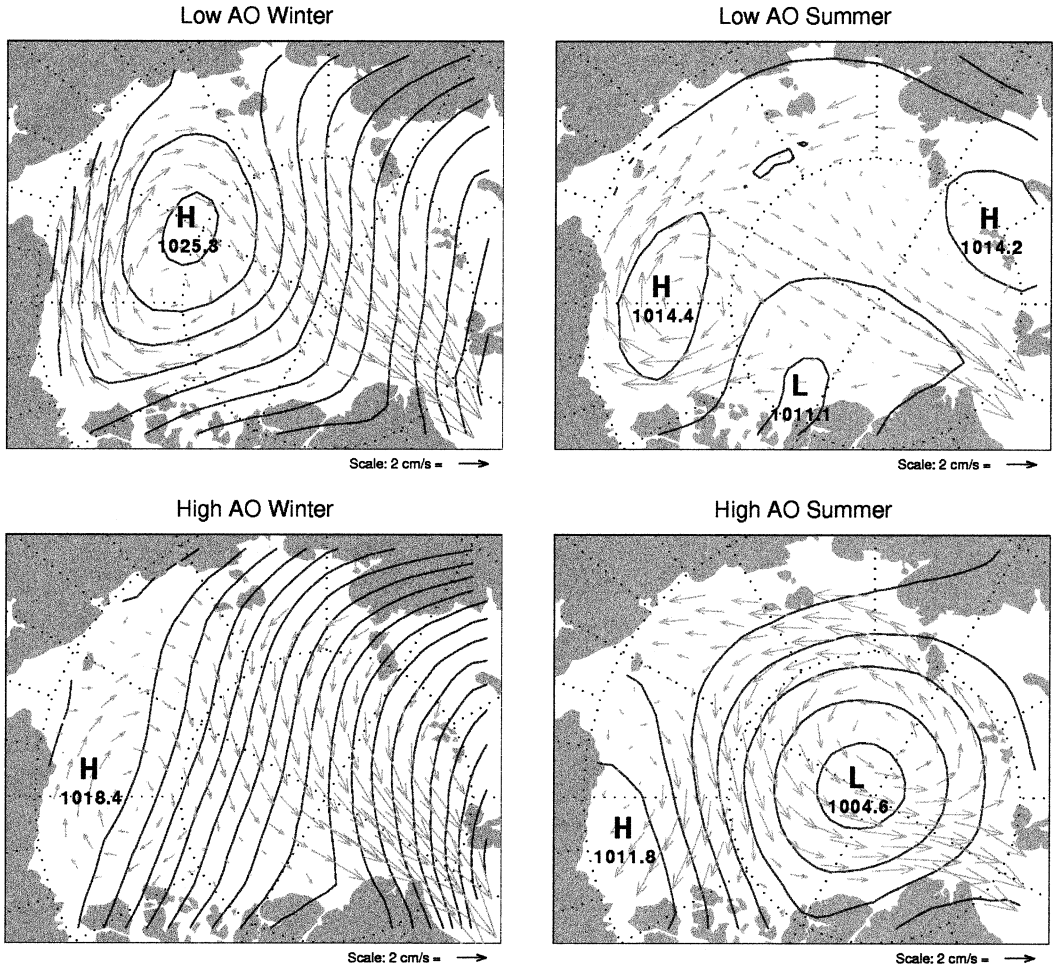

FIG. 9. Composite maps of AO SLP and SIM: (left) winter, (right) summer, (top) low index, and (bottom) high index.

low-index phase. We assume that these minor differences are due simply to the significant increase in observations now available. Given that all studies of these regimes presume them to be associated with different atmospheric circulation patterns, and the fact that the AO is the dominant mode of variability of atmospheric circulation, then the striking correspondence between the two representations suggests that the contrasting regimes in SIM noted by Gudkovich (1961) correspond closely to the low and high phases of the AO.

6. Impact of changes in SIM on sea ice thickness, the surface heat budget, SIC, and SAT on large scales

Notable changes at the surface of the Arctic Ocean during the past few decades include the warming of SAT (Rigor et al. 2000), the thinning of sea ice (Rothrock et al. 1999), and the summertime decrease in the area covered by sea ice (Parkinson et al. 1999). One could ask, did the warming of SAT act to thin and decrease the area of sea ice, or did the thinner and less expansive area of sea ice allow more heat to flux from the ocean to warm the atmosphere? The Arctic is a complex system with many feedbacks, but if the thickness and area of sea ice were reduced due to a trend toward warmer SAT, then one would expect to observe an increase in the advection of heat over the Arctic Ocean during this period. Thompson and Wallace (2000) show in their Fig. 11 the anomalous advection of heat associated with the AO. This figure clearly shows that the warming over Eurasian landmasses can be attributed to warm advection. However, over the ocean, their pattern shows cold advection, consistent with the strengthening of the surface winds from the interior of Eurasia (e.g., Figs. 5c, 6c, and 8), the coldest region of the Northern Hemisphere, toward the Arctic Ocean. Apparently, other processes must have caused the warming of SAT over the Arctic Ocean.

We have shown that the trend toward a more cyclonic circulation over the Arctic, or equivalently, toward the positive polarity of the AO, has clearly influenced sea

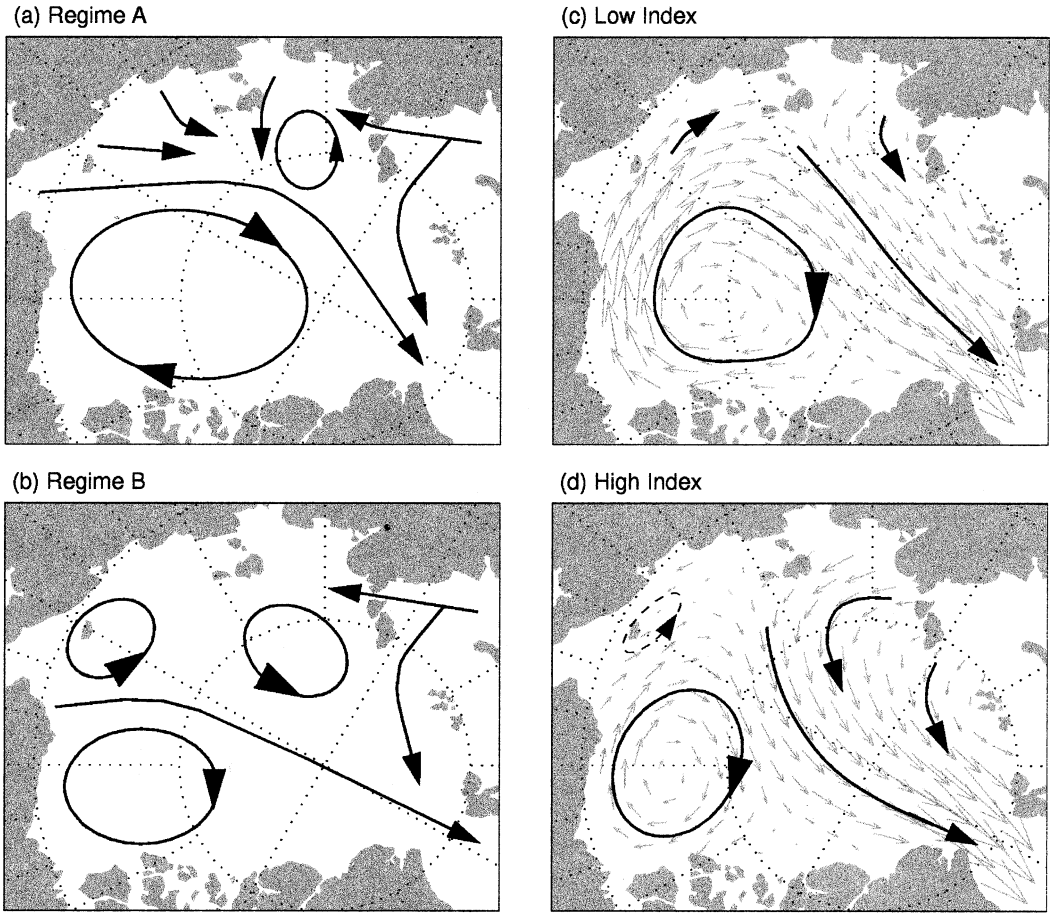

FIG. 10. (a), (b) Regimes of ice motion described by Gudkovich (1961), and circulations of ice during (c) low-index and (d) high-index phases of the AO index.

ice motion. We now consider how the changes in sea ice motion might have affected sea ice thickness, the surface heat budget, sea ice concentration, and surface air temperature.

a. Thinning of Arctic sea ice

During the high-index phase of the AO, the cyclonic anomaly in SIM implies increased divergence of sea ice due to Ekman transport at the sea surface to the right of the wind forcing. This divergence should enhance the formation of new ice in the open leads during winter, and thus enhance the flux of heat from the ocean. The decreased convergence in the reduced, anticyclonic Beaufort gyre implies less ridging and less recirculation of ice. Both these processes should contribute to the thinning of sea ice over the Arctic Ocean.

Figure 11 shows isochrone maps of the mean number of years that it would take ice along various trajectories to be advected through the Fram Strait under low- and high-index conditions. The dashed line near the edge of the Beaufort gyre in these figures marks the boundary separating ice that would be advected through Fram Strait from ice that would be recirculated in the Beaufort gyre by the mean SIM field. These figures show that mean residence time for ice in the Beaufort gyre is >5 yr, but it takes on ~ 1 yr for ice at the North Pole to drift to Fram Strait.

Comparing the low-index to the high-index map (Figs. 11a and 11b), it is evident that during high-index conditions, ice in the Beaufort gyre takes a year longer to be advected from the west to the east Arctic than during low-index conditions, and ice passing over the North Pole reaches Fram Strait more quickly during high-index conditions. The decrease in advection of ice from the western to the eastern Arctic and the increase in ice drift from the pole toward Fram Strait during high-index conditions are also evident in the regression maps of ice motion upon the AO. These results are consistent with an increase in the divergence of ice associated with the cyclonic anomaly in SIM in the eastern Arctic.

Quantitative estimates of the divergence of sea ice were obtained by estimating the amount of ice advecting from the western to the eastern Arctic, and from the Arctic Ocean through Fram Strait (see appendix). During low-index years, 0.6×10^6 km^2 of ice is transported

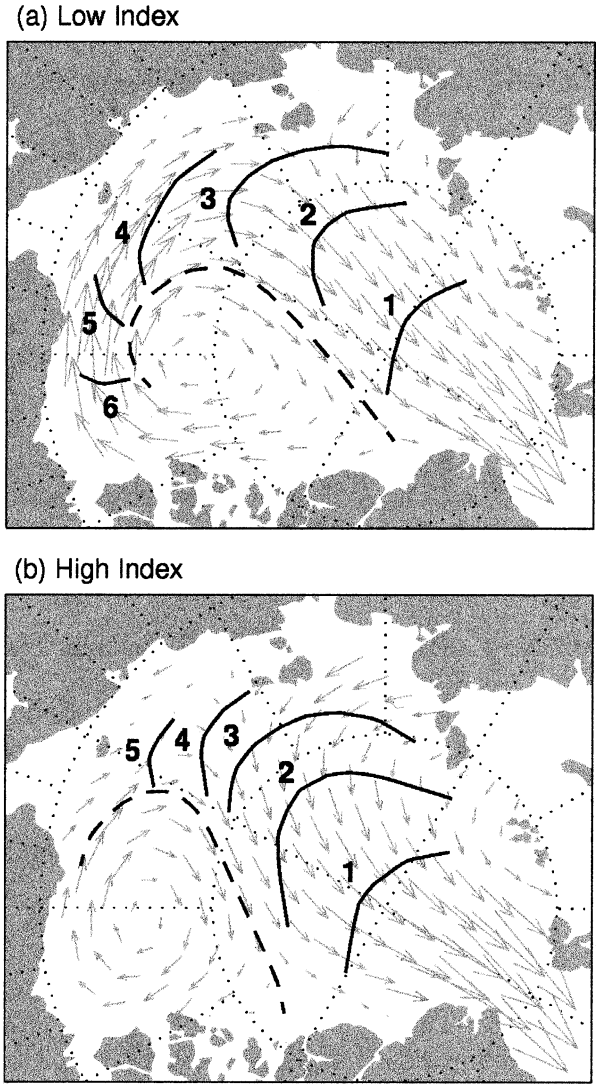

FIG. 11. Isochrone maps showing the number of years required for a parcel of ice to exit from the Arctic through Fram Strait. (a) Field during the low-index phase of the AO index and (b) field during high-index phase of AO. The dashed line delimits the area for which ice either recirculates in the Beaufort gyre or is advected through the Fram Strait.

from the western to the eastern Arctic, and 0.9×10^6 km^2 of ice exits through Fram Strait. During high-index years the areal flux from the western to the eastern Arctic all but vanishes, while there is a 10% increase in the flux through Fram Strait. Divergence of sea ice increases by 13% over the Arctic as a whole, and doubles in the eastern Arctic.

Figure 11b also shows stronger SIM away from the East Siberian and Laptev Seas in the high-index phase of the AO. During winter, this advection away from the coast opens up a flaw lead (a crack in the ice) along the fast ice edge in which new ice can form. Rigor and Colony (1997) estimated that in the mean as much as 20% of the ice area transported through Fram Strait is produced in the flaw leads of the Laptev Sea. Given the increased advection away from the coast during the high-index phase of the AO, it can be inferred that production of new thin ice in the flaw leads of the East Siberian and Laptev Seas should increase. This process also contributes to the thinning of sea ice over the Arctic Ocean.

An increased areal flux through Fram Strait does not necessarily imply a higher volume flux. During the low-index phase of the AO, a significant portion of the ice flowing toward Fram Strait originates from the Beaufort gyre where it may recirculate longer and thus become thicker before it exits through Fram Strait. During the high-index phase, a larger area of ice is transported through Fram Strait, but much of this ice originates in the East Siberian and Laptev Seas or is formed by the increased divergence of ice in the eastern Arctic and is most likely younger, thinner multiyear ice. These changes might account for at least part of the thinning of Arctic sea ice reported by Rothrock et al. (1999).

b. Trends in surface air temperature and sea ice concentration

The surface heat budget of the Arctic Ocean is dominated by radiative fluxes, but the exchange of heat between the Arctic Ocean and atmosphere is strongly moderated by the thickness of sea ice. For example, during winter the sensible and latent heat flux into the atmosphere from a refreezing open lead is $\sim$700 W m^{-2}, as compared to $\sim$10 W m^{-2} into the ocean over 3 m thick (Maykut 1978). Although leads compose only $\sim$1% of the ice pack at any given time, these turbulent heat fluxes exceed the radiative fluxes. These leads quickly freeze over, but only grow to $\sim$0.4 m thick after a week (Ono 1967), at which thickness they still release $\sim$80 W m^{-2} into the atmosphere (Maykut 1978). Young ice of intermediate thickness (0.2–0.8 m), which is estimated to compose 8%–12% of the ice pack (Wittmann and Schule 1966), is believed to exert the greatest influence on the flux of heat into the atmosphere (Maykut 1982). It takes new ice over a month to grow thicker than 1 m (Ono 1967), at which thickness the heat fluxes drop to less than 30 W m^{-2} into the atmosphere (Maykut 1978), but during the growth of sea ice from open water to 1-m-thick ice, $\sim$200 MJ m^{-2} are released to the atmosphere (Maykut 1982). Averaged over a month, this implies an average heat flux of 77 W m^{-2} into the atmosphere. Most of the heat transferred from the Arctic Ocean to the atmosphere is concentrated in these leads and thin ice (Badgley 1966; Maykut 1982; Aagaard and Carmack 1994). Processes that increase the amount of open water and thin ice may have a significant impact on the flux of heat from the Arctic Ocean to the atmosphere and may have a strong effect on SAT.

Warming trends in SAT have been noted over the Arctic Ocean by Rigor et al. (2000) during winter and spring. The spring trends were found to be significant

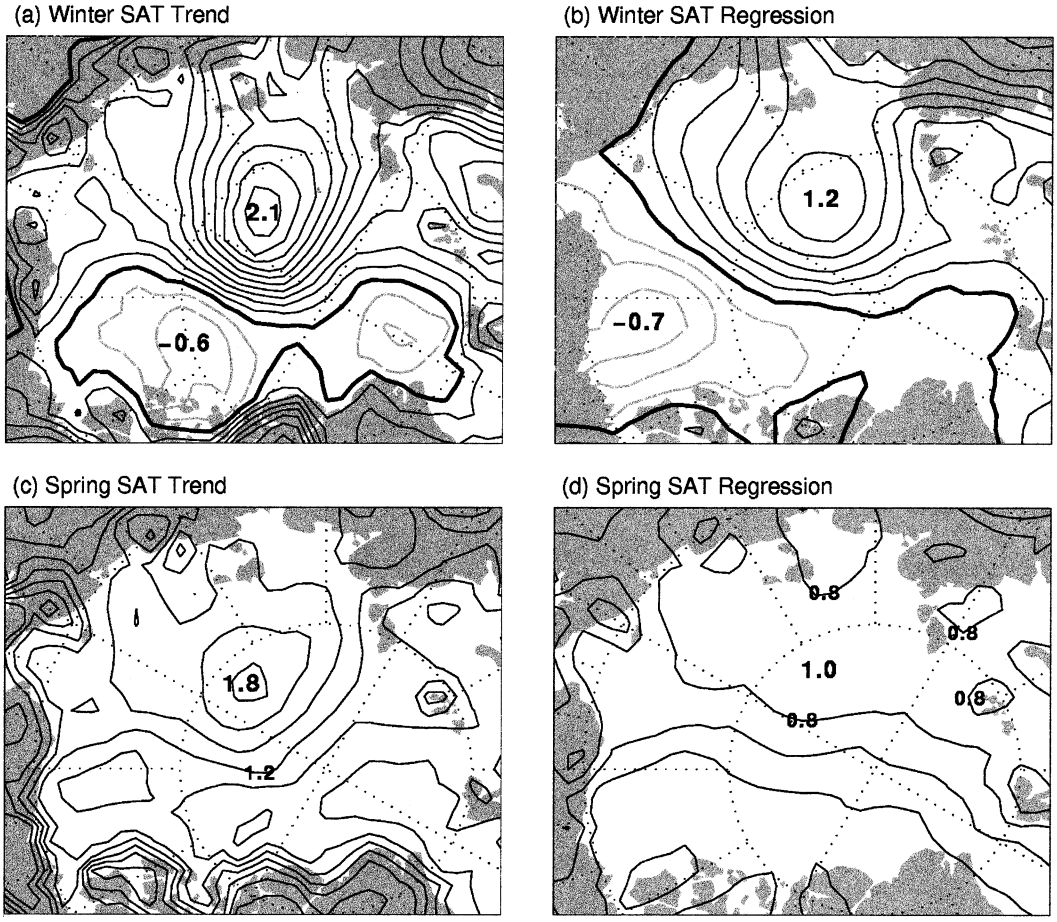

FIG. 12. Winter (NDJFM) SAT (a) trends and (b) regression on the winter AO. (c),(d) Same as (a) and (b) except for spring (AM) SAT. Contours are shown every 0.2°C decade^{-1}.

at the 99% confidence level. Rigor et al. (2000) also showed that the wintertime SAT trends exhibit a spatial pattern similar to the anomalies associated with the AO and are largely attributable to the trend in the AO.

The anomalies associated with the high-index phase of AO (Fig. 8a) show increased advection of sea ice away from the coast, and a cyclonic anomaly in SLP and SIM, which should enhance the divergence of sea ice in the eastern Arctic. Both of these processes should favor the formation of more leads and increase the production of thin ice during winter. We estimate that the production of new sea ice during winter in the eastern Arctic increases from 155 000 km^2 during low AO winters to 357 000 km^2 during high AO winters (Table A1, appendix). Since leads and thin ice contribute more than half of the flux of heat from the ocean to the atmosphere over the Arctic Ocean, and the amount of new thin ice more than doubles from low to high AO winters, we infer that the heat flux from the ocean to the atmosphere should increase by more than 50% from low to high AO years, which is in agreement with the warming of SAT over the eastern Arctic.

Using a coupled sea ice–ocean model, Zhang et al. (2000) studied the changes in sea ice thickness. In part of their study they forced the model with interannually varying winds, but fixed the SAT to only have an annual cycle. They found that ~80% of the thinning of sea ice could be attributed to dynamic affects on the sea ice driven by the NAO, that is, increased advection away from the coast, and the cyclonic anomaly in ice motion both act to increase the production of thin ice during winter. Although feedbacks from the sea ice–ocean to the atmosphere were not accounted for in their model, it can be inferred that at least part of the warming that has been observed is due to the heat released during the increased production of new ice, and the increased flux of heat to the atmosphere through the larger area of thin ice.

Figures 12a and 12c show the winter and spring trends in SAT from 1979 to 1998. The seasons in these figures are defined as the cold months of winter (NDJFM), the summer months (JJA) when SAT throughout the Arctic tends to be uniform and close to the freezing point, and the transition seasons spring (AM) and fall (SO). Figures 12b and 12d show regressions of the winter and spring seasonal mean SAT on the seasonal mean wintertime

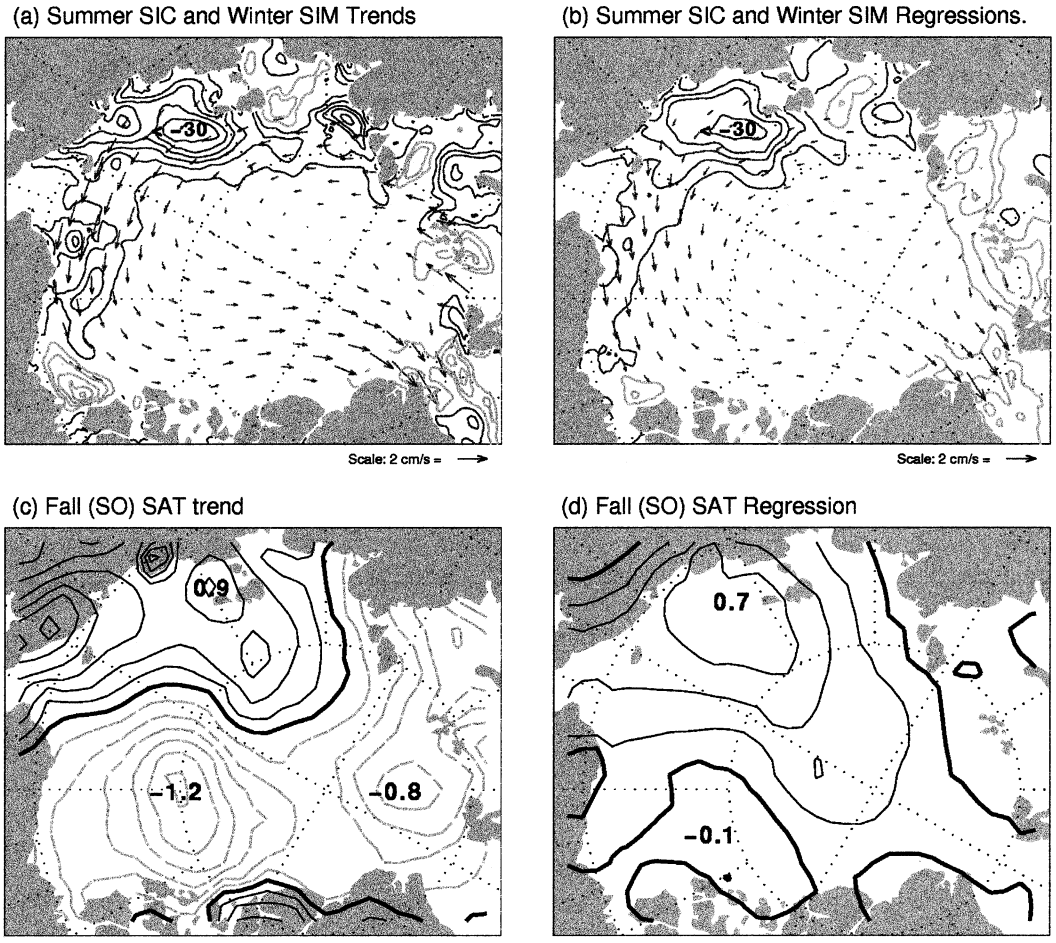

FIG. 13. (a) Large-scale trends in summer SIC and winter SIM. (b) Regression of summer SIC on the prior winter AO. (c),(d) Fall (SO) SAT trends and regression on the winter AO. Contours are shown every 5% decade^{-1}. Dark contours indicate decreasing trends.

AO. As shown here and in Rigor et al. (2000), the regression of wintertime SAT on the AO accounts for most of the trends in winter SAT over most of the Arctic. Regressing seasonal mean springtime SAT on the seasonal mean AO for the previous winter yields regression coefficients in excess of 0.7°C decade^{-1}, which are statistically significant at the 95% confidence level based on a two-sided Student's t-test with 13 degrees of freedom and a null hypothesis of zero correlation. Both the trend and the regression patterns for spring exhibit pronounced warming over the eastern Arctic, but less in the western Arctic. This signal is not evident in the regression of spring SAT upon the spring AO (not shown). We attribute these significant correlations to the memory provided by sea ice; that is, during winter, the AO drives the dynamic thinning of sea ice, rendering it a weaker insulator, allowing more heat flux to pass from the ocean, and raising the SAT. The warmer temperatures, together with the fact that first year ice melts at lower temperatures because it is saltier, brings on an earlier onset of melt.

Changes in wintertime SIM also appear to be at least partially responsible for the trends in summer SIC and extent noted by Parkinson et al. (1999). Figure 13a shows the summer trends in SIC from the SSM/I–SMMR data for 1979–98 superimposed on the trends in SIM from the previous winter. The trends in summer SIC are consistent with the changes in winter SIM. Specifically, significant trends toward decreasing SIC are found during summer. These trends are largest in the East Siberian Sea where the trends in wintertime SIM are toward less packing of ice and increased advection away from the coast. Figure 13b shows summer mean SIC regressed upon the seasonal mean AO index from the previous winter, together with previous winter SIM regressed upon the concurrent winter AO index. These patterns are remarkably similar to the trends in summer SIC and winter SIM (Fig. 13a). The lagged regressions between summer SIC and the previous winter AO also agree with modeling studies (e.g., Bitz 1997; Walsh and Zwally 1990), which support the notion that ice thick-

ness during summer in the Siberian Arctic is preconditioned by wintertime conditions.

During summer, the lower SIC areas also exhibit lower albedos, which increases the amount of insolation absorbed. Then in the fall, the extra heat stored by the ocean and the larger mass of open water delays the onset of freezing, and more heat is released to the atmosphere during the cooling and freeze up.

The summer trends toward decreasing SIC (Fig. 13a) and the trends toward warmer autumn SAT trends (Fig. 13c) exhibit similar patterns; that is, the largest warming trends in autumn occur in the area of the largest decreases in summer SIC. We have shown that during summers following low AO winters, the marginal seas of the eastern Arctic tend to be covered with sea ice, but following high AO winters, there are large expanses of open water (Figs. 13a,b). During the autumn freeze up following a high AO winter, the large expanse of summer open water cools and then freezes up. Since the area of the East Siberian Sea is $\sim$1 000 000 km^2, and SIC decreases $\sim$50% from low to high AO years, we estimate that $\sim$500 000 km^2 more new ice is produced during high AO years, which allows $\sim$200 MJ m^{-2} of heat to flow into the atmosphere and explains the autumn warming trend. The autumn trends also resemble the regressions upon the previous winter AO index (Figs. 13c,d). It is notable that the largest warming trends in autumn coincide with the area of the largest decreases in summer SIC.

The regressions of seasonal SAT and summer SIC shown here partly reflect the correlation associated with the trend in both datasets and the AO. However, the AO remains significantly correlated with the seasonal SAT and summer SIC when the trend is removed and the regression patterns do not change qualitatively (not shown).

Hilmer and Jung (2000) note a secular change in the relationship between the Fram Strait ice flux and the NAO; the high correlation noted by Kwok and Rothrock (1999) from 1978 to 1996 was not found in data prior to 1978. We expect our overall results to be more robust given the strong relationship between the AO and SIM over the Arctic, as compared to the weaker relationship between the north–south flow through Fram Strait and the AO. Even if one ignored the effect of the AO on the flux of ice through Fram Strait, the divergence of sea ice in the eastern Arctic would be still be $\sim$50% greater under high-index conditions than under low-index conditions, and the heat flux would be $\sim$25% greater.

Comparable results were obtained by regressing the summer SIC trends upon the winter mean NAO (not shown), but the features are not as strong. The NAO explains only 36% of the variance in SIC in the eastern Arctic, whereas the AO explains 64%.

Regressions of summer SIC on the summer AO yields a pattern that may explain some of the changes in summer SIC in the Beaufort Sea, but does not exhibit the most prominent features of the observed trends in summer SIC such as the large decreases in SIC in the eastern Arctic.

7. Impact of changes in SIM on SIC on small scales

Figure 14 shows the changes in the summer SIC in the Russian marginal seas in greater detail. Increasing SIC are found in the eastern parts of the East Siberian, Laptev, and Kara Seas, and lower SIC are found in the western parts of those seas. These changes are consistent with the cyclonic trends (eastward drift) in SIM during all seasons.

The small-scale trends in SIC can be explained as follows. In the East Siberian Sea, the summer trends show decreases in SIC, which are larger on the western shores than to the east. During low-index years, the stronger Beaufort gyre packs ice into the East Siberian Sea; this ice rafts and thickens. However, during high-index years when the Beaufort gyre shrinks, the circulation in the East Siberian Sea is marked by strong advection away from the fast ice (i.e., ice that is ''fixed'' in location and is a persistent wintertime feature in the shallow shelf areas of these seas) during winter, which produces more than ice. The fast ice edges shown in Fig. 14 mark the seaward limit of the 90% SIC during winter as estimated from the SIGRID ice chart data. When the ice melts during spring and summer, the concentrations are much lower for thinner new ice than for the thicker rafted ice that may have been recirculating in the Beaufort gyre for a number of years. The ice that remains in the sea during summer is advected eastward by the wind-driven SIM, which is stronger during high-index years and was stronger during the second decade of the record. The Laptev and Kara Seas also exhibit a decreasing ice concentration adjacent to the fast ice edge on the western side, and increasing concentration on the eastern side, consistent with the trend toward stronger eastward SIM during summertime.

8. Conclusions

Increased advection of ice away from the coast during winter during high-index conditions of the AO enhances the production of thin ice in the flaw leads of the East Siberian and Laptev Seas. The cyclonic SIM anomaly also enhances the production of thin ice during winter because of the increase in divergence over the eastern Arctic. Both of these processes contribute to the thinning of sea ice. These changes in SIM have contributed to the observed trends in sea ice, such as the decreases in ice area and extent, and the thinning of sea ice.

The changes in SIM also appear to be at least partially responsible for the trends in SAT reported by Rigor et al. (2000); that is, the increased latent heat released during the formation of new ice in the diverging leads, and the increased heat flux through thinner ice have

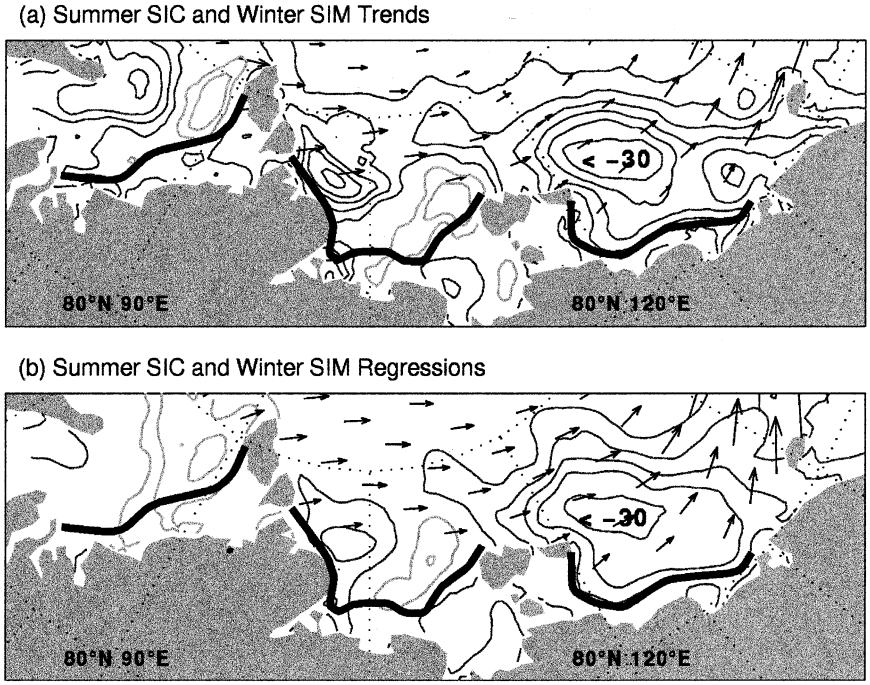

FIG. 14. (a) Small-scale trends in summer SIC and winter SIM in the Russian marginal seas. (b) Regression of summer SIC on the prior winter AO. Contours are shown every 5% decade^{-1}. Dark contours indicate decreasing trends. The thick black lines show the extent of fast ice from the coast.

contributed to the pronounced warming that has been observed in the East Siberian and Laptev Sea portions of the warm anomaly. Intuitively, one might have expected the warming trends in SAT to cause the thinning of sea ice, but the results presented in this study imply the inverse causality; that is, that the thinning ice has warmed SAT by increasing the heat flux from the ocean.

We have shown that sea ice provides memory for the Arctic climate system so that changes in SIM driven by the AO during winter can be felt during the ensuing seasons; that is, the AO drives dynamic thinning of the sea ice in the eastern Arctic during winter, allowing more heat to be released from the ocean through the thinner ice during spring, and resulting in lower SIC during summer and the liberation of more heat by the freezing of the ice in autumn. The correlations between the wintertime AO and SIC and SAT during the subsequent seasons offers the hope of some predictability, which may be useful for navigation along the Northern Sea route.

Acknowledgments. The authors wish to thank the participants of the International Arctic Buoy Programme who maintain the Arctic buoy network. The data from this program have been essential in detecting many of the changes in Arctic climate noted in this paper. We would like to thank D. Battisti, C. M. Bitz, D. A. Rothrock, and J. Zhang for their helpful discussions, and M. Ortmeyer for computer assistance. We would also like to thank J. Walsh for his thoughtful and insightful review, which has greatly strengthened this paper.

Rigor is funded by a fellowship from the Applied Physics Laboratory, University of Washington, and by the U.S. Interagency Buoy Program under ONR Grant N00014-98-1-0698. Wallace is funded by the National Science Foundation under Grant ATM 9850886. Colony is supported by the Frontier Research System for Global Change.

APPENDIX

Estimating the Areal Flux and Divergence of Sea Ice

Estimates of areal flux and divergence are important for the mass balance of sea ice, the freshwater balance of the Arctic Ocean, and it has implications for the driving of the global thermohaline circulation. In order to estimate how they are impacted by the AO, we calculate the areal flux through Fram Strait and from the Chukchi to East Siberian Seas (western to eastern Arctic, across 180° longitude from 72° to 80°N). These ''gates'' are the lines across which we would expect to see the most pronounced effect of the AO upon the areal flux.

The gate at Fram Strait is defined following Kwok and Rothrock (1999), who estimate ice flux from microwave data along the 400-km line between the north-

TABLE A1. Areal ice flux (10^3 km^2 per season).

Fram Strait	Winter	Spring	Summer	Autumn	Annual
Low index	260	207	169	287	923
High index	363	250	164	273	1050
Western to eastern Arctic	Winter	Spring	Summer*	Autumn*	Annual*
Low index	105	202	70	225	611
High index	6	50	−68	45	33
Eastern Arctic net	Winter	Spring	Summer*	Autumn*	Annual*
Low index	155	5	99	62	312
High index	357	200	232	228	1017

* These estimates may be high during some years, since the summer minimum ice edge varies from 70° to 76°N along 180°.

west tip of Svalbard and Antarctic Bay at the northeast tip of Greenland. We assume 100% SIC and estimate the areal flux as the product of the gate width and the average displacement of ice for each season perpendicular to the gate. To account for the coastal effects (Kwok and Rothrock 1999), we also reduce our estimates through Fram Strait by 10%. Between the western and eastern Arctic, we define the flux gate as the line from 72° to 80°N along 180° and assume no coastal effects. It should be noted, however, that the concentration of ice during summer and autumn in this area is highly variable. Using the SIC data we find that although the mean minimum ice edge (50% SIC) at the end of summer (mid-September) is at about 72°N at 180°, the minimum ice edge varies from 70° to 76°N.

Compared to Thorndike and Colony (1982), who estimated areal ice flux through Fram Strait using buoy data from the early, low-index years of the buoy program, our estimates of ice flux during low-index years are comparable. Compared to Kwok and Rothrock (1999), our estimates are on average 27 000 km^2 higher during all seasons, and 68 000 km^2 higher for the annual average. These differences may simply be due to small differences in the locations of our gates in Fram Strait, where there is a large gradient in SIM.

Table A1 shows the average areal ice flux through both gates for each season. In the mean, ice advects through Fram Strait during all seasons, peaking during winter (311 000 km^2) and reaching a minimum during summer (167 000 km^2). The ice advection from the western to eastern Arctic, across 180° peaks during autumn (135 000 km^2), but the errors during this season are rather large due to the fact that SIC in this area is actually much less than 100% during summer and autumn. Hence we may be overestimating the flux by as much as 50% during summers and autumns when the SIC is low. We believe that the ice flux estimates from the western to eastern Arctic are more robust during winter and spring.

During high-index years, the ice flux through Fram Strait is 10% higher than low-index years. Most of this difference is attributable to winter. Across 180°, the ice flux from the western to eastern Arctic all but vanishes during high-index years.

The net areal flux of ice into the eastern Arctic can be estimated by taking the difference between the net flux of ice into the eastern Arctic from the west across 180°, and the ice leaving the eastern Arctic through Fram Strait. Compared to low index, ice flux increases through Fram Strait during high-index winter and spring, and decreases across 180° during all seasons. The increase in flux through Fram Strait and the much larger decrease in flux across 180° can also be seen in Figs. 9, 10, 11. This implied divergence is consistent with the cyclonic anomaly in SLP and SIM. In the mean there is a net export of 670 000 km^2 from the eastern Arctic. The net export from the eastern Arctic ranges from 312 000 km^2 during low-index years to 1 017 000 km^2 during high-index years. Most of the sea ice in the central Arctic basin exits through Fram Strait. Hence SIM in the Arctic Ocean is essentially ''divergent.'' Estimates of this divergence can be obtained by simply dividing the areal fluxes shown in Table A1 by the respective areas. Specifically, the flux through Fram Strait, divided by the total area of the Arctic Ocean ($\sim 6.5 \times 10^6$ km^2), yields an estimate of the divergence for the entire Arctic. Likewise, the divergence averaged over the western Arctic can be estimated from the flux of ice from the western to the eastern Arctic, and the divergence over the east can be estimated from the net flux out of that area. For the estimates of divergence in the western and eastern Arctic, the definition of these areas is important. Although one may choose to define them geographically (e.g., by east and west longitudes), a better way may be by inspection of the mean fields of SIM, considering the changes in SIM related to the AO. For our estimates of divergence, we define the western Arctic as the area bounded by the gate from the western to the eastern Arctic, and the boundary line for which ice will recirculate in the Beaufort gyre (Fig. 11). The areas for the western and eastern Arctic vary depending on the phase of the AO. During low index, the areas of the western and eastern Arctic are 1.5×10^6 km^2 and 5.0×10^6 km^2, respectively, and during high index the areas are 1.0×10^6 km^2 and 5.5×10^6 km^2, respectively.

Table A1 shows the flux of sea ice over the Arctic Ocean. For the whole basin, we see that the annual mean

divergence is about 0.042% day^{-1}, and the changes in divergence related to the AO are small (0.005% day^{-1}). However, the changes in divergence for the western and eastern Arctic are larger. In the west, the divergence decreases from 0.110% day^{-1} during low index to 0.009% day^{-1} during high index, and in the east, the divergence increases from 0.018% day^{-1} during low-index to 0.051% day^{-1} during high-index conditions. The divergence in the eastern and western Arctic can be related to the whole by multiplying the divergence estimates for each region by the area covered in each region, divided by the whole area. These estimates agree with the expected increase in divergence in the eastern Arctic associated with the cyclonic anomaly in SIM, and the decrease in convergence in the western Arctic associated with the reduced area of the Beaufort gyre.

REFERENCES

Aagaard, K., 1989: A synthesis of the Arctic Ocean circulation. *Rapp. P.-V. Reun. Cons. Int. Exploration de la Mer,* **188,** 11–22.

——, and E. C. Carmack, 1994: The Arctic Ocean and climate: A perspective. *The Polar Oceans and Their Role in Shaping the Global Environment: The Nansen Centennial Volume,* O. M. Johannessen, R. D. Muench, and J. E. Overland, Eds., Amer. Geophys. Union, 5–20.

Badgley, F. I., 1966: Heat balance at the surface of the Arctic Ocean. *Proc. Symp. on the Arctic Heat Budget and Atmospheric Circulation,* Santa Monica, CA, Rand Corporation, 215–246.

Bitz, C. M., 1997: A model study of natural variability of the Arctic Climate. Ph.D. dissertation, University of Washington, 200 pp.

Colony, R., and A. S. Thorndike, 1984: An estimate of the mean field of Arctic sea ice motion. *J. Geophy. Res.,* **89** (C6), 10 623–10 629.

Gudkovich, Z. M., 1961: Relation of the ice drift in the Arctic basin to ice conditions in the Soviet Arctic seas (in Russian). *Tr. Okeanogr. Kom. Akad. Nauk SSSR,* **11,** 14–21.

Hilmer, M., and T. Jung, 2000: Evidence for a recent change in the link between the North Atlantic Oscillation and Arctic sea ice export. *Geophys. Res. Lett.,* **27,** 989–992.

Hurrell, J. W., 1995: Decadal trends in the North Atlantic Oscillation: Regional temperatures and precipitation. *Science,* **269,** 676–679.

Kwok, R., and D. A. Rothrock, 1999: Variability of Fram Strait ice flux and North Atlantic oscillation. *J. Geophys. Res.,* **104** (C3), 5177–5189.

Leith, C. E., 1973: The standard error of time-average estimates of climatic means. *J. Appl. Meteor.,* **12,** 1066–1068.

Maykut, G. A., 1978: Energy exchange over young sea ice in the central Arctic. *J. Geophys. Res.,* **83** (C7), 3646–3658.

——, 1982: Large-scale heat exchange and ice production in the central Arctic. *J. Geophys. Res.,* **87** (C10), 7971–7984.

Ono, N., 1967: Specific heat and heat of fusion of sea ice. Vol. 1, *Physics of Snow and Ice,* H. Oura, Ed., Inst. Low Temp. Sci., Hokkaido, Japan, 599–610.

Parkinson, C. L., D. J. Cavalieri, P. Gloersen, H. J. Zwally, and J. Comiso, 1999: Arctic sea ice extents, areas, and trends, 1978–1996. *J. Geophys. Res.,* **104** (C9), 20 837–20 856.

Pfirman, S. L., R. Colony, D. Nürnburg, H. Eichen, and I. Rigor, 1997: Reconstructing the origin and trajectory of drifting Arctic sea ice. *J. Geophy. Res.,* **102** (C6), 12 575–12 586.

Proshutinsky, A. Y., and M. A. Johnson, 1997: Two circulation regimes of the wind-driven Arctic Ocean. *J. Geophys. Res.,* **102** (C6), 12 493–12 514.

Rigor, I. G., and R. L. Colony, 1997: Sea-ice production and transport of pollutants in the Laptev Sea, 1979–1993. *Sci. Tot. Environ.,* **202,** 89–110.

——, ——, and S. Martin, 2000: Variations in surface air temperature observations in the Arctic, 1979–97. *J. Climate,* **13,** 896–914.

Rothrock, D. A., Y. Yu, and G. A. Maykut, 1999: Thinning of the Arctic sea-ice cover. *Geophys. Res. Lett.,* **26,** 3469–3472.

Thompson, D. W. J., and J. M. Wallace, 1998: The Arctic oscillation signature in the wintertime geopotential height and temperature fields. *Geophys. Res. Lett.,* **25,** 1297–1300.

——, and ——, 2000: Annular modes in the extratropical circulation. Part I: Month-to-month variability. *J. Climate,* **13,** 1000–1016.

Thorndike, A. S., and R. Colony, 1982: Sea ice motion in response to geostrophic winds. *J. Geophys. Res.,* **87,** 5845–5852.

Walsh, J. E., and H. J. Zwally, 1990: Multiyear sea ice in the Arctic: Model- and satellite-derived. *J. Geophys. Res.,* **95,** 11 613–11 628.

——, W. L. Chapman, and T. L. Shy, 1996: Recent decrease of sea level pressure in the central Arctic. *J. Climate,* **9,** 480–485.

Wittmann, W. I., and J. J. Schule, 1966: Comments on the mass budget of arctic pack ice. *Proc. Symp. on the Arctic Heat Budget and Atmospheric Circulation,* Santa Monica, CA, Rand Corporation, 215–246.

Zhang, J., D. Rothrock, and M. Steele, 2000: Recent changes in the Arctic sea ice: The interplay between ice dynamics and thermodynamics. *J. Climate,* **13,** 3099–3114.

Zubov, N. N., 1943: Arctic ice (in Russian). Glavsevmorputi, 360 pp. (English translation, Transl. 103, U.S. Navy Electr. Lab., San Diego, CA.)